J. Comp. App. Res. Mech. Eng. Vol. 13. No. 2, pp. 137-156, 2024 *DOI: 10.22061/JCARME.2024.10107.2352*

Journal of Computational and Applied Research in Mechanical Engineering

jcarme.sru.ac.ir

SRTTU

JCARME

ISSN: 2228-7922

Research paper

A comprehensive numerical investigation of the effects of inlet operating conditions on the performance of 3-fluid liquid-to-air membrane energy exchangers

Aydin Zabihi and Nader Pourmahmoud*

Mechanical Engineering Department, University of Urmia, Urmia, Iran

Article info:

Article history:

Received: 04/08/2023

Accepted: 30/01/2024

Revised: 02/02/2024

Online: 04/02/2024

Keywords:

3-fluid LAMEE,

Semi-permeable membrane,

Heat and mass transfer,

Refrigeration tube,

Air dehumidification.

***Corresponding author:**

n.pormahmoud@urmia.ac.ir

Abstract

3-fluid liquid-to-air membrane energy exchangers (LAMEEs) are economic dehumidification systems. Cooling tubes are put into dehumidifier liquid channels to regulate the internal temperature of the dehumidifier liquid. 3D computational fluid dynamics is used to simulate a 3-fluid LAMEE, and extra transfer of both heat and mass formulas, along with the essential equations that govern viscous fluid flow, are compiled using external computer programs known as UDS (User Defined Scalar). This study thoroughly investigates the impact of water inflow variables on system efficiency. The refrigeration fluid that runs inside the cooling tubes is water. The temperature distribution of the three fluids is investigated and the role of the refrigeration tubes based on their positions is evaluated on the desiccant solution cooling. Six tests are conducted to achieve the best arrangement of the inlet water conditions based on the tube's geometrical location. At an intake water mass flow rate of 4.67 g/s, the latent and sensible effectiveness rise from 51% to 78% and 60% to 130%, respectively, when the input water temperature drops from 24.6 °C to 10.1 °C.

1. Introduction

Buildings are known as the main consumers of energy and dehumidification has a significant portion in energy consumption [1–4]. Hence, recently much research has been conducted to decrease the consumption of energy in HVAC systems. Desiccant dehumidification systems that were originally launched had a significant impact on reducing energy usage, but they still had some carry-over issues with the liquid desiccant into the buildings because they were in close touch with the air streams [5, 6].

After that, LAMEEs were created that utilize membranes with the airflow and the dehumidifier liquid, eliminating the direct contact between both streams. The membranes allow both moisture and heat to travel through the airflow and the desiccant solution without getting mixed.

The drawback of this kind of dehumidification system is that as the temperature rises, the dehumidifier liquid's absorption decreases. To

that end, Abdel-Salam *et al*. [7] designed a unique prototype of a 3-fluid LAMEE in which cooling tubes were put into the dehumidifier solution, and a refrigerant was utilized to chill it. They discovered that when contrasted to a 2-fluid LAMEE with comparable factors, the total, sensible, and latent efficiency, sensible cooling capacity and moisture removal rate of the 3-fluid LAMEE raised to 39%, 69%, 28%, 140%, and 54%, respectively.

The critical point is that in 3-fluid LAMEEs, the cooling of the dehumidifier liquid and, hence, the operation of the system, are greatly impacted by the refrigeration tubes. To this end, the effects of the inlet water conditions are comprehensively studied the temperature distribution of the three fluids is analyzed, and the influence of the seven refrigerant tubes is geometrically examined in this paper. The purpose of the present work is to find the best inlet conditions to achieve the maximum performance of the system.

Min Tu *et al.* [8] designed and formulated a renewable ventilating system with two packed columns for dehumidification and regeneration and they examined how important the parameters affected how well the system performed. Zhang [9] introduced the progress of research on membrane-based heat and moisture recovery when utilized as an airflow drier and diluting dehumidifier liquid regenerated. Mohammad Abdel-Salam *et al.* [10] showed how a flat-plate LAMEE's steady-state efficiency may be adjusted to humidity and solution channel thicknesses.

A computer simulation of combined warmth and moisture transmission in a run-around heat transfer system employing a liquid dehumidifier and fluid was created by Seyed-Ahmadi *et al.* [11].

A computational framework for two-dimensional structures in a steady state was developed by Vali *et al.* [12]. The mobility of the liquid and thermal conduction transfer of mass in membrane-formed identical panel channels was investigated by Si-Min Huang *et al.* [13]. According to Jafarian *et. al.* [14], who evaluated dehumidifier performance under various inlet air conditions, the designed indoor dehumidifier is the most effective one. Hongu Bai *et al.* [15] used calcium chloride to test the efficiency of a membrane-based fluid adsorbent dehumidifying technology. They examined how critical operating parameters, the total, sensible, and latent efficacy of dehumidification are influenced by factors including the number of heat transfer units (NTU) and the humidity-to-dehumidifier-liquid mass flow rate ratio (m*). Experimental research was done by Storle *et al.* [16] to examine the efficiency of a 3-fluid LAMEE cooling system.

Kabeel [17] carried out an experiment to assess the effectiveness of a dehumidifier liquid framework for dehumidifying and humidifying using fresh air. The desiccant framework was studied under a variety of working settings, including varying temperatures, humidity ratios, and solution levels. According to the CFD model published by Alipour *et al.* [18], with an equivalent sensible cooling capacity, the suggested LAMEE has roughly 25–28% less saturation than the standard LAMEE.

The distributions of frost and condensation are significantly impacted by the variations in humidity ratio, as demonstrated by Alipour *et al.* [19]. The best way to prevent icing is to alter both the humidity and temperature ratio so that air moisture does not exceed absorption levels. Xia Song *et al.* [20] studied the best configuration of pf area partition among packing towers across the same overall area in liquid desiccant dehumidifier mechanisms. A lot of research has been done on LAMEEs but they have studied either the impacts of their construction and design and functioning on the efficiency of the system experimentally [12, 21–25] or they formulated equations that govern both moisture and heat transmission [10, 26–28]. According to research by Bartuli *et al.* [29], the total heat exchange efficiency for cross-wound PHFHE with an exterior water flow rate of 0.08 m/s was 1170 W/m^2K at a hollow fiber water temperature of 11°C and an outer shell liquid temperature of 70°C.

These days, absorbent membrane energy converters are very important because dehumidification using absorbents uses a very small amount of energy when compared to traditional air conditioning systems, and semi-permeable porous membranes have solved the

issues caused by the absorbent coming into direct contact with air. Many experimental attempts have been made in recent years to improve the effectiveness and operating conditions of these kinds of systems, but research that can fully simulate this system using computational fluid dynamics and explain the mechanisms of simultaneous heat and moisture transfer has consistently been lacking. There was a thorough examination. As a result, this study comprehensively investigated the process of the simultaneous transmission of humidity and heat from the air to the absorber and refrigerant, which used the computational fluid dynamics technique and Ansys Fluent simulation software to simulate the three-flow model of these converters. The internal temperature of the absorbent liquid in the 3-fluid idea is controlled with water flowing via chilly tubes located within the absorbent solution channel. Since increasing the inlet operation efficiency of these tubes and channels (air and solution) enhances the overall performance of absorption membrane energy converters, our research aims to achieve this fundamental goal.

Throughout the investigations that have been done, computational fluid dynamics (CFD) has not been used in 3-fluid LAMEEs studies so far. Furthermore, there are various difficulties in reproducing conjugate heat and moisture transport phenomena in a 3-fluid LAMEE, including the requirement to calculate extra mass and heat transfer equations. To completely represent the laws of physics of fluid flows, external software programs (UDS) are used in this mechanical system.

2. The definition of the 3-fluid LAMEE model

Fig. 1 depicts the blueprint of the 3-fluid LAMME constructed by Abdel-Salam *et al*. [7]. This research proposes a CFD simulation that uses the experimental framework. As seen, the model is a flat plate 3-fluid LAMEE, and the air stream flows through two channels located on both sides of a desiccant solution channel. Seven titanium refrigerant tubes are positioned in the desiccant solution channel and water runs through them, which comes into proximity with the desiccant solution.

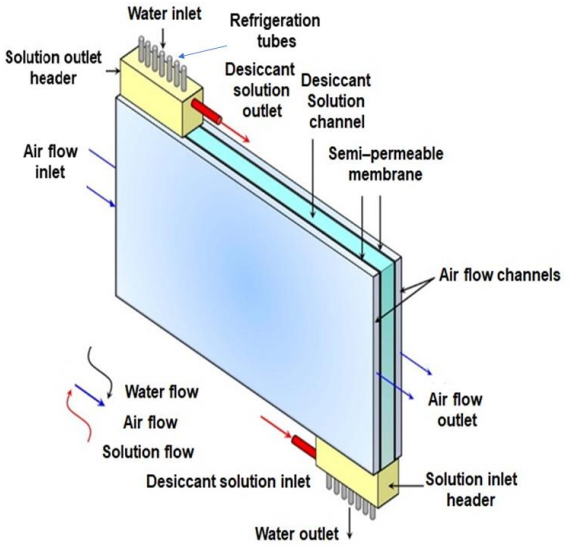

Fig. 1. Blueprint of the 3-fluid LAMEE [7].

The dehumidifier liquid comes through the solution inlet header and departs through the solution outlet header located at the top of the system. Dehumidifier and air channels are partitioned by microporous membranes that are semi-permeable with a 55% porosity (30 nm pore diameter).

The desiccant solution is made of an aqueous solution of 32.5% lithium chloride (LiCl). Conde [30], discovered the properties of aqueous lithium chloride solutions. The 3-fluid LAMEE measurements and their inlet boundary parameters are shown in Tables 1 and 2, respectively. The boundary conditions, which are based on Abdel-Salam's experimental work, are demonstrated in Table 2 [7].

The air channel's mass flow rate is 1.19 g/s, the inlet temperature is 35.1 °C, and the inlet humidity ratio is 17.6 g_v/kg_{air}. Temperatures in the refrigeration tubes channel range from 10.1 °C to 24.6 °C, with intake flow rates of 1.22 g/s to 9.35 g/s. LiCl concentration is 32.5 g/s, and the inlet mass flow rate is 0.76 g/s for the solution channel.

Fig. 2 shows the CFD model of the 3-fluid LAMEE used in the present work. The model was created using ANSYS ICEM CFD (ver. 17.2) and STAR CCM+ (Ver. 12), and the fluid mechanics flow in the three-fluid LAMEE was computed using ANSYS Fluent.

Table 1. Synopsis of the 3-fluid LAMEE parameters utilized in Rashidzadeh CFD simulation [31].

Case	Parameter	Value	Unit
Exchanger	Flow configuration (solution-air)	Counter-cross	-
	Flow configuration (solution-refrigerant)	Counter	-
	Length	470	mm
	Height	100	mm
	Exchanger aspect ratio (height/length)	0.31	-
	Exchanger solution entrance ratio	0.11	-
	Nominal air channel width	5	mm
	Nominal solution channel width	4.2	mm
	Number of air channels	2	-
	Number of solution channels	1	-
	Mass (empty)	1.71	kg
Membrane	Thickness	0.3	mm
	Mass resistance (R_m)	38	s/m
	Liquid penetration pressure	124	kPa
Refrigeration tubes	Refrigerant	Water	-
	Tube material	Titanium	-
	Number of tubes	7	-
	Tube length	660	mm
	Inner diameter	2.362	mm
	Outer diameter	3.175	mm
	Wall thickness	0.4	mm
	Spacing between tubes	9.7	mm
	Thermal conductivity	21	(W/(m·k))

Table 2. An overview of the 3-fluid LAMEE's input boundary conditions.

LAMEE	Input parameter	Value	Unit
Air	Temperature, $T_{air,in}$	35.1	℃
	Humidity ratio, $W_{air.in}$	17.6	g_v/kg_{air}
	Mass flow rate	1.19	g/s
Solution	Temperature, $T_{sol,in}$	24.8	℃
	Concentration, C_{sol}	32.5	%
	Mass flow rate	0.76	g/s
Water	Temperature, $T_{w,in}$	10.1, 15.1, 20.4, 24.6	℃
	Mass flow rate	1.22, 1.98, 4.67, 9.35	g/s
Design and operating parameters	NTU	1.8	-
	Cr^*	1.8	-
	Cr	0.055, 0.11, 0.26, 0.42	-

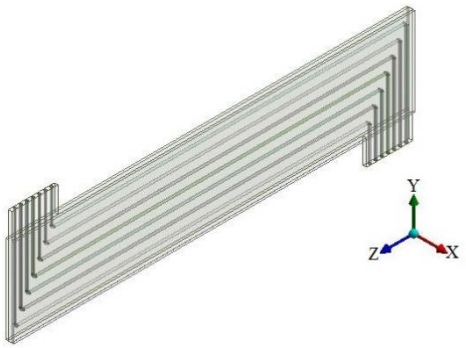

Fig. 2. CFD model of the 3-Fluid LAMEE with 7 refrigeration tubes.

3. Assessment of LAMEEs' effectiveness

A LAMEE's performance can be assessed using the moisture removal rate ($\dot{m}_{rr}$) measures and effectiveness (ε) [32].

3.1. Effectiveness (ε)

A LAMEE's effectiveness is divided into three categories: latent, total, and sensible. Sensible effectiveness (ε_{sen}) is a proportion of the actual to the highest feasible rates of sensible heat

transfer in the LAMEE. The discrepancy between the real and the highest practicable water transfer rates is referred to as latent effectiveness (ε_{lat}).
The ratio of the actual to the maximum feasible rates of energy transfer (enthalpy) is known as total effective-ness (ε_{tot}). Eqs. (1-3) are used to determine the sensible effectiveness, latent effectiveness, and total effectiveness of a solution with a heat capacity more than the air heat capacity (Cr^*≥1).

$$E_{sen} = \frac{T_{air,in} - T_{air,out}}{T_{air,in} - T_{sol,in}} \quad (1)$$

$$\varepsilon_{lat} = \frac{W_{air,in} - W_{air,out}}{W_{air,in} - W_{sol,in}} \quad (2)$$

$$\varepsilon_{tot} = \frac{\varepsilon_{sen} + H^{*}\varepsilon_{lat}}{1 + H^{*}} \quad (3)$$

In the given example, $T_{air.in}$ represents the temperature of the entrance air (℃), $T_{air.out}$ represents the temperature of the exhaust air (℃) and $T_{sol.in}$ represents the temperature of the entrance desiccant solution (℃). The air humidity ratio is kg_v/kg_{air}, whereas the air humidity ratio at the outflow is $W_{air.out}$. The equilibrium humidity ratio of the salt solution at the inlet is $W_{sol.in}$ (kg/kg). The operational variable, H^*, can similarly be found using Eq. (4) [33].

$$H^{*} = \frac{\Delta H_{lat}}{\Delta H_{sen}} \approx 2500 \frac{W_{air.in} - W_{sol.in}}{T_{air.in} - T_{sol.in}} \quad (4)$$

3.2. Moisture removal rate (Dehumidification rate) ($\dot{m}_{rr}$)

A further important consideration in determining a LAMEE's performance is the moisture removal rate, which is the rate at which moisture is transferred from the air to the streams of desiccant solution, as shown by Eq. (5).

$$\dot{M}_{rr} = \dot{m}_{air} |W_{air,out} - W_{air,in}| \quad (5)$$

where $\dot{m}_{air}$ is the mass flow rate of the inlet air (kg/s).

3.3. Sensible cooling capacity (SCC)

The cooling capacity of a LAMEE can be measured by the efficiency of the thermal exchange with airflow and the dehumidifier solution.

$$SCC = \dot{m}_{air} c_{p,air} (T_{air,in} - T_{air,out}) \quad (6)$$

where $c_{p.air}$ denotes the air's specific heat capacity (J/kg.K).

3.4. Design parameters

A LAMEE's efficiency is dictated by the following design parameters: NTU, NTU_m, Cr^*. Cr, $C_{sol,\ in}$.

3.4.1. Number of heat transfer units (NTU)

A LAMEE's practical effectiveness is greatly influenced by the quantity of thermal transfer units (NTU) [7, 34].

$$NTU = \frac{UA}{C_{min}} \quad (7)$$

$$U = \left[\frac{1}{h_{air}} + \frac{\delta}{k_{mem}} + \frac{1}{h_{sol}}\right]^{-1} \quad (8)$$

Air's convection coefficient of heat transfer (h_{air}), which is measured in (W/m^2. K), is represented by U (W/m^2K). The membrane thickness is δ (m). The membrane total area is A (m^2), the minimal rate of thermal conductivity for streams of dehumidifier solution is C_{min} (W/K).
Thermal conductivity of the membrane (k_{mem}) is measured in units of (W/m.K) and the desiccant solution's convective heat transfer coefficient is h_{sol} and is measured in (W/m.K).

3.4.2. Number of mass transfer units (NTU_m)

Transfer of mass units is connected with the latent performance of a LAMEE of which the following definition holds:

$$NTU_m = \frac{U_m A}{\dot{m}_{min}} \quad (9)$$

$$U_m = \left[\frac{1}{h_{m,air}} + \frac{\delta}{k_m} + \frac{1}{h_{m,sol}}\right]^{-1} \quad (10)$$

The overall mass transfer coefficient is U_m (kg/m^2 s) and the humidity and desiccant solution's minimum mass flow rate is $\dot{m}_{min}$ (kg/s). The air's convective mass transfer coefficient is represented by the symbol $h_{m.air}$ (kg/m^2 s), The desiccant solution's convective mass transfer coefficient is $h_{m.sol}$ (kg/m^2 s) and the unit of measurement for membranes permeability of fluid is k_m (kg/m/s).

3.4.3. Heat capacity ratios ($Cr^*. Cr$)

The desiccant solution's heat capacity rates to air flows are measured as Cr^*. Cr refers to the ratio of the dehumidifier and refrigeration fluid's lowest and highest heat capabilities.

$$Cr^* = \frac{C_{sol}}{C_{air}} = \frac{\dot{m}_{sol}\, c_{p.sol}}{\dot{m}_{air} c_{p.air}} \tag{11}$$

$$Cr = \frac{C_{min}}{C_{max}} = \frac{C_{sol}}{C_{ref}} = \frac{\dot{m}_{sol}\, c_{p.sol}}{\dot{m}_{ref} c_{p.ref}} \tag{12}$$

The desiccant solution's $C_{p,\,sol}$ is its specific heat capacity (j/kg. k) and $C_{p,\,air}$ stands for the air's specific heat capacity and the refrigerant's specific heat capacity is expressed as $C_{p,\,ref}$ (j/kg. k). The mass flow rate of the solution is expressed as $\dot{m}_{sol}$ (kg/s) and the refrigerant's mass flow rate is expressed as $\dot{m}_{ref}$ (kg/s).

3.4.4. Concentration of desiccant solution ($C_{sol,\,in}$)

Dehumidifier liquid concentration is defined as the ratio of desiccant mass to an aqueous solution.

$$C_{sol,in} = \frac{\text{mass of desiccant}}{\text{mass of desiccant} + \text{mass of water}} \tag{13}$$

4. Governing equations

It is thought that the three-dimensional, 3-fluid LAMEE has a steady state, laminar flows. The essential laws controlling the behavior of fluid flow are as follows: the following is the mass conservation formula, also referred to as continuity Eq. (14).

$$\frac{\partial \rho}{\rho t} + \nabla \cdot (\rho \vec{v}) = S_m \tag{14}$$

According to [35, 36] the source word S_m refers to any user-defined sources as well as the mass contributed to the permanent phase through the distributed subsequent phase (for instance, as a result of vapor transfer through the membrane).

$$\frac{\partial}{\partial t}(\rho \vec{v}) + \nabla \cdot (\rho \vec{v}\vec{v}) = -\nabla p + \nabla \cdot (\bar{\bar{\tau}}) + \rho \vec{g} + \vec{F} \tag{15}$$

The momentum equation is given by [35, 36] Eq. (15), where p denotes static pressure, denotes stress tensor, $\bar{\bar{\tau}}$ and $\rho\vec{g}$ and $F^{\rightarrow}$ represent the system forces of gravity and the outside, respectively. $\vec{F}$ is made up of extra conceptions about porous medium that are defined by user sources and rely on models. The energy formula is solved by ANSYS Fluent in the following way:

$$\frac{\partial}{\partial t}(\rho E) + \nabla \cdot \left(\vec{v}(\rho E + p)\right) = \nabla \cdot \left(K_{eff} \nabla T - \sum_j h_j \vec{J}_j + (\bar{\bar{\tau}}_{eff} \cdot \vec{v}) \right) + S_h \tag{16}$$

K_{eff} stands for effective conductivity, and the species j's diffusion flux is denoted by $\vec{J}_j$. Energy transfer resulting from conduction, species diffusion, and viscous dissipation is each represented by one of the first three terms on the right. $E = h - \frac{p}{\rho} + \frac{v^2}{2}$ and $h = \sum_j Y_j h_j$ are similarly applicable.

The computer fluid dynamics (CFD) study of the current energy converter is particularly challenged by the extra formulas of both moisture and heat transmission from the humidity surroundings to the dehumidifier liquid. Because having a semi-permeable membrane with specific qualities like thickness, porosity, and permeability has a significant impact on the computing process.

In this process, moisture is moved from the ambient air flow to the dehumidifier solution. The solution-membrane channel contact heats two fluids, and heat is released when the transported water changes phases. The desiccant

solution contains vapor. The previously mentioned elements must additionally involve harvesting of the diffusing and absorption processes. [12, 35, 36].
The law of conservation of mass yields the following when considering water vapor in the atmosphere:

$$\frac{2U_m y_0}{m_{air}}(W_{air} - W_{sol}) = -\frac{\partial W_{air}}{\partial x} \quad (17)$$

The total transfer of mass ratio U_m. W_{air}, is dependent upon temperature and relative humidity is the air's humidity ratio. It is the connection between the amount of dry air and the amount of liquid moisture in the atmosphere;

$$W_{air} = \frac{\text{mass } H_2O}{\text{mass Air}} = f(\emptyset_{air}. T_{air}). \quad (18)$$

W_{sol}, a function of temperature and salt content in the solution, is the humidity ratio of the air in an equilibrium with the salt solution; $W_{sol} = f(X_{sol}. T_{sol})$.
According to Hemingson *et al.* [37], Eq. (17) is correct because W_{sol}, $W_{sol,membrane}$ and transport of humidity is not very hampered on the solution portion.
Regarding the liquid side, water mass preservation is taken into consideration:

$$2U_m(W_{air} - W_{sol}) = \rho_{salt} d_{sol}(u_{sol}\frac{\partial X_{sol}}{\partial x} + v_{sol}\frac{\partial X_{sol}}{\partial y}) \quad (19)$$

where X_{sol} is the mass of water in the saltwater mixture and is the proportion of the total weight of liquid to the weight of pure brine;

$$X_{sol} = \frac{\text{Mass } H_2O}{\text{Mass Pure Salt}}. \quad (20)$$

One way to express energy conservation in the air side is as follows:

$$\frac{2Uy_0}{C_{air}}(T_{air} - T_{sol}) = -\frac{\partial T_{air}}{\partial x} \quad (21)$$

where $C_{air} = \dot{m}_{air}\, c_{p.air}$ and the general thermal transfer efficiency is denoted by U.
Related energy conservation on the liquid side is:

$$2U(T_{air} - T_{sol}) + 2U_m h_{fg}(W_{air} - W_{sol}) = (\rho c_p d)_{sol}(u_{sol}\frac{\partial T_{sol}}{\partial x} + v_{sol}\frac{\partial T_{sol}}{\partial y}) \quad (22)$$

where $2U_m h_{fg}(W_{air} - W_{sol})$ is the energy released as a result of the water vapor's phase change.
The additional Eqs. (17–22) describe how to represent the process of the thermal and humidity exchange mechanism in a 3-fluid LAMEE. There is no easy way to tackle these in the ANSYS FLUENT software. Therefore, exterior software called UDS (User Defined Scalar) must be used in conjunction with any CFD simulation in this field.

5. Grid independence study

As illustrated in Fig. 3, a three-dimensional grid system was set for numerical calculations. Additionally, a thorough research of grid independence was carried out to find the appropriate grid resolution and eliminate numerical mistakes from computations. As a result, various mesh types, ranging from coarse to dense were taken into consideration. Accordingly, with initial temperature of water 10.1 °C and Cr=0.26 circumstances, the major criteria were outlet air temperature (°C) and outlet air humidity ratio (g_v/kg_{air}).

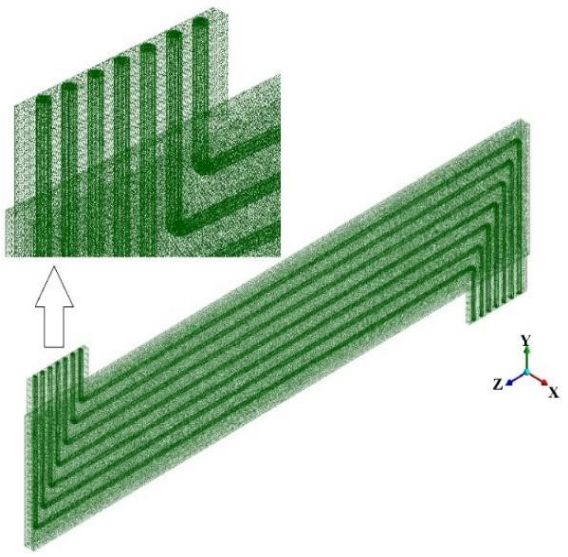

Fig. 3. 3-fluid LAMEE grid system.

As seen in Fig. 4, stage A's outlet air temperature and stage A's outlet air humidity ratio fluctuate as the number of elements increases while remaining more or less constant in stage B. To minimize the amount of meshes with different mesh sizes for each of the seven tubes, their thickness, the air channels, membranes, and solution channel have been separately meshed in the STAR-CCM+ software and assembled inside Ansys Fluent. Consequently, a domain with 2527542 items was chosen.

6. Validation

Since Abdel-Salam et al.'s laboratory research served as the basis for the design and testing of the numerical simulation used in this study [7], the results were validated using experimental data with similar design circumstances and procedures.

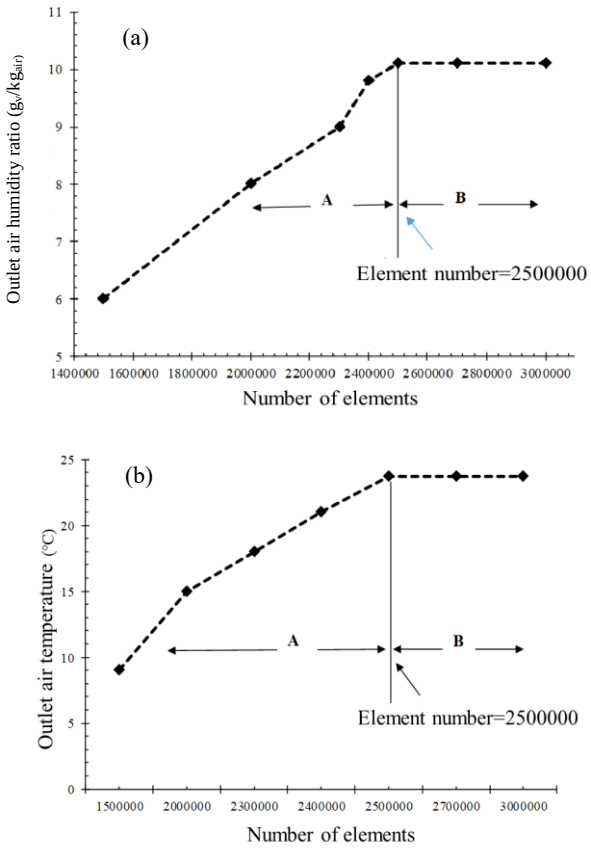

Fig. 4. Grid independence analysis based on (a) humidity ratio, and (b) temperature criteria of the outlet air (Cr=0.26, $T_{w,in}$=10°C).

To validate the numerical results with the experimental results, the experimental data was used to assess the CFD-based outputs of the air outlet's temperature and moisture proportion. Heat capacity rate ratio (Cr) was kept 0.26 and the inlet water temperature changed from 10.1°C to 24.6°C. Tables 1 and 2 show the measurements and inlet boundary conditions, respectively. Table 3 shows both the experimental data and the computational findings for the 3-fluid flow LAMEE. As can be observed, the current study's results are in excellent alignment with the actual data, with only minor differences due to the numerical calculations and experimental correlations. Fig. 5 shows comparisons between the present results and the experimental data.

7. Results and discussion

A refrigerant as third fluid is used in 3-fluid LAMEEs to cool the desiccant solution, and roughly keeps the temperature of the desiccant solution constant. Due to this, water conditions (such as temperature and mass flow rate) have a substantial impact on desiccant solution cooling. In the present study, the effects of water conditions on the system efficiency are examined comprehensively in the following sections. Furthermore, the impacts of refrigerant tubes on their placements are explored and the ideal inlet water conditions for different tubes are introduced.

Table 3. Comparison of numerical and experimental results for 3-fluid LAMEE

Parameter		Experimental in laboratory	Computational fluid dynamic analysis	Variations (%)
	Unit	Value	Value	Value
$T_{water,\ out}$	°C	16.2	18.61	14.8
$T_{solution,\ out}$	°C	23.7	24	1.3
$T_{air,\ out}$	°C	23.9	23.1	3.3
$W_{air,\ out}$	g_v/k	9.95	10.1	1.5
ε_{sen}	%	112.8	116.5	3.2
ε_{lat}	%	65.9	67.5	2.4
ε_{tot}	%	78.6	80.8	2.8
$\dot{m}_{rr}$	g_v/h	29.98	32.13	7.2
SCC	W	13.5	14.35	6.3

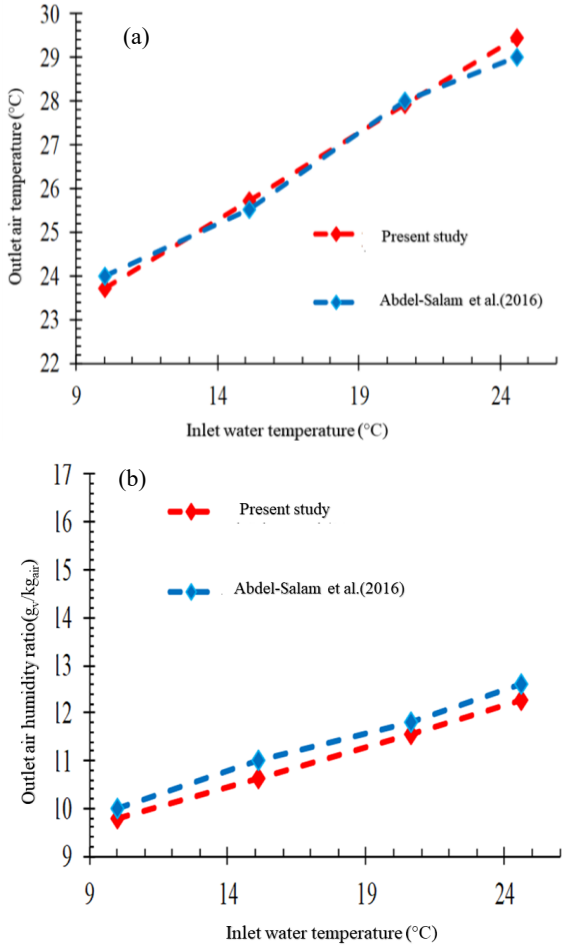

Fig. 5. Validation of present study with experimental data base on (a) outlet air temperature and (b) outlet air humidity ratio.

7.1. Effect of inlet water temperature

The differences in the latent, total, and sensible effectiveness and the moisture removal rate with the inlet water temperature $T_{w,in}$ under different inlet water mass flow rates are investigated. As seen in Fig. 6, they all behave similarly to decrease the initial freshwater temperatures and they grow as the initial freshwater temperatures fall under varying mass flow rates.

The impact of initial water temperatures on the dehumidifier liquid relates to its cooling role. This raises the mixture's temperature as warmth is transmitted from the transition phases to the dehumidifier liquid via the air flow and then into the desiccant solution. In other words, when the inlet water temperature decreases, it can cool down the dehumidifier liquid more.

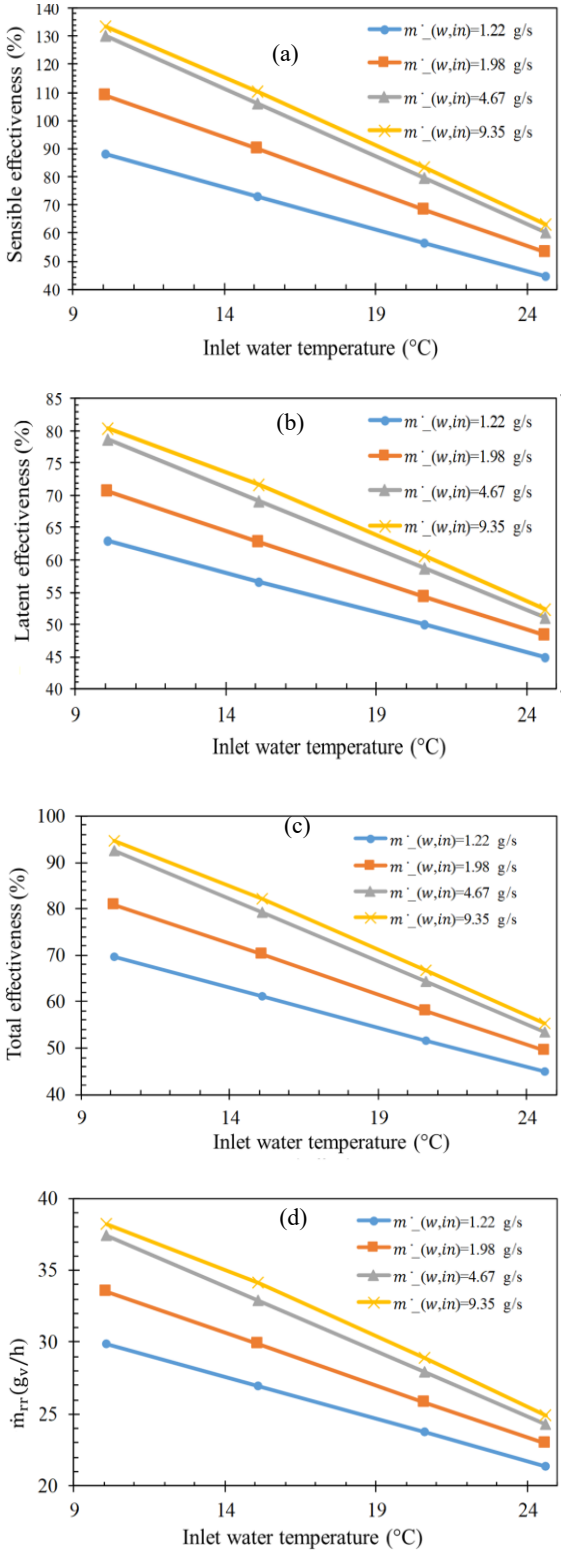

Fig. 6. Variations of (a) sensible effectiveness, (b) latent effectiveness, (c) total effectiveness, and (d) moisture removal rate with inlet water temperature under different inlet mass flow rates.

As a result, the total temperature of the dehumidifier liquid falls, but the difference in temperature through the airflow and the dehumidifier liquid rises, suggesting that thermal exchange between the two streams may occur and potentially increasing sensible efficiency.

For instance, at the inlet water mass flow rate of 4.67 g/s, the sensible effectiveness increases from 60% to 130% as the temperature of the entering water drops from 24.6 °C to 10.1 °C.

Furthermore, when the variance between the vapor pressures within the airflow and the dehumidifying liquid widens, the likelihood of humidity transfers between the two airflow and the dehumidifier liquid increases.

Consequently, the latent effectiveness and the moisture removal rate rise. The latent effectiveness and the moisture removal rate increase from 51% to 78% and 24 g_v/h to 37 g_v/h, respectively, when the temperature of the initial water drops from 24.6 °C to 10.1 °C at the inlet water mass flow rate of 4.67 g/s.

According to Eq. (3), the overall efficacy of the system is governed by the sensible and latent efficiency; consequently, the overall efficacy improves as the incoming freshwater temperatures drops. The initial intake water's ambient temperature drops from 24.6 °C to 10.1 °C, resulting in an increase in total effectiveness from 53% to 92% at the inlet water mass flow rate of 4.67 g/s, as shown in Fig. 6(c).

Hemingson demonstrated how the efficacy rates depend a great deal on the external environment, with certain efficiency rates reaching 100% or falling below 0% for a number of the examined external conditions of air [37].To determine the impact of the initial water thermal (as the 3rd liquid) on the two other fluids (the desiccant solution and the air stream), the temperature variation across the exchanger is examined.

Therefore, at first horseshoe-type temperature profile is described by Fig. 7, then the effect of different inlet water temperatures is analyzed (Fig. 8). The variation in temperature on the XZ axis at $\dot{m}_{w.in} = 1.98\ g/s$. $T_{w.in}$ =10.1 °C and at the center of tube 4 (y=81.95 mm) is depicted in Fig. 7(a) and Fig. 7(b) showing the profile of temperature across the plane at Z/L=0.8.

As seen in Fig. 7(a), heat is transferred through the airflow to the dehumidifier liquid, and the temperature of the airflow steadily drops. Meanwhile, the water absorbs the heat delivered to the dehumidifier liquid as well as the heat released during the phase shift, and its warmth grows as it travels throughout the refrigeration tubes. In Fig. 7(b), the tube's center is A, the water stream runs from A to B, the tube's thickness is B to C, the desiccant solution is C to D, and the membrane and air stream are D to E. The temperature of the center of the tube is minimum and the temperature increases as it moves from the center of the tube toward the outer layers of the air stream (from A to E).

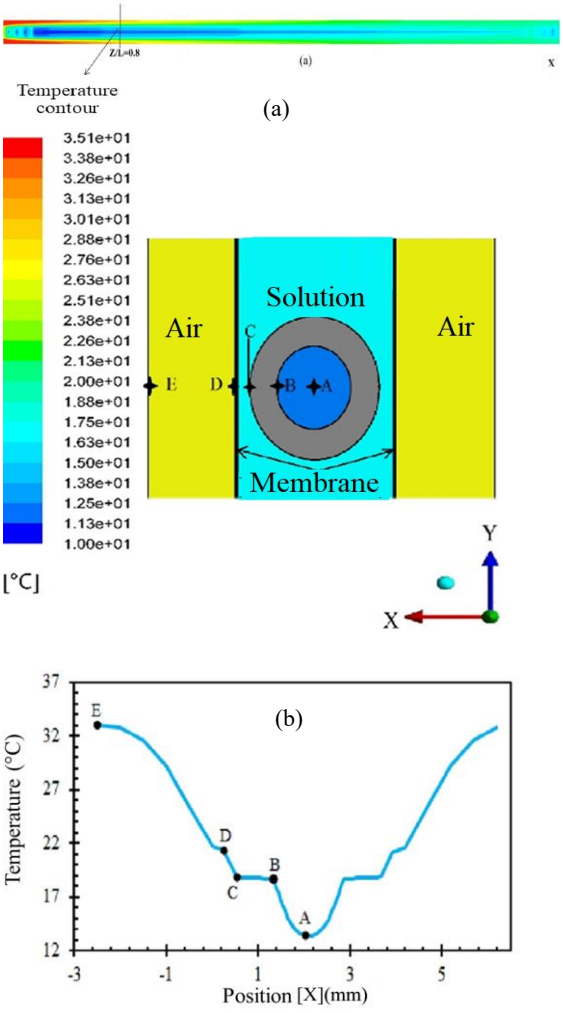

Fig. 7. (a) Temperature distribution on the XZ plane at tube 4 (y=81.95 mm), (b) temperature profile throughout the plane at Z/L=0.8.

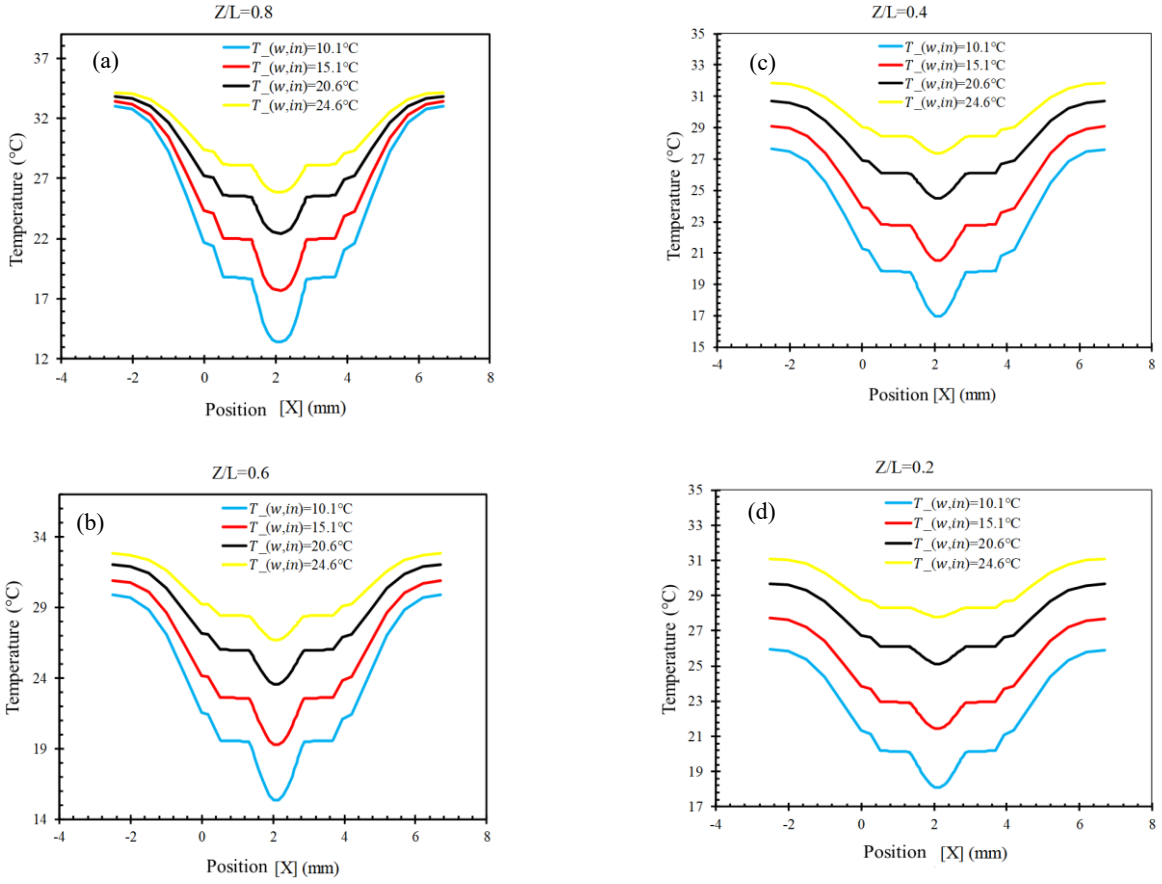

Fig. 8. Variations of temperature across the XZ plane at (a) Z/L=0.8, (b) Z/L=0.6, (c) Z/L=0.4, and (d) Z/L=0.2 under different inlet water temperatures

Fig. 8 displays the variations of temperature across the XZ plane (at the center level of tube 4) at different Z/L under different inlet water temperatures and $\dot{m}_{w.in}$=1.98 g/s. The tube's center temperature drops as the entrance water temperature drops between 24.6 °C to 10.1 °C, consequently the temperatures of the dehumidifier liquid and the airflow decrease.

At Z/L=0.8 (the location nearest the air entrance), the outer layers of the air stream do not have enough time to transfer heat to the inner layers and the temperatures of the air stream (D-E) at different air inlet temperatures are very close (Fig 8(a)). The further we get air from the inlet, the hotter the center of the tube becomes through taking up the desiccant solution's thermal. For example, the temperature of the center of the tube increases from 13°C at Z/L=0.8 to 18°C at Z/L=0.2 where $T_{w,\,in}$=10.1°C

Furthermore, as one approaches the air exit, the temperature differential between the air streams increases due to the differing inlet water temperatures.

As seen in Fig. 8, the temperature of the desiccant solution (C-D in profiles) approximately remains constant by the refrigeration tubes, for example at $T_{w,\,in}$=10.1 °C, the variation of the solution temperature ranges from 20°C to 21°C at Z/L=0.2 and 19 °C to 21°C at Z/L=0.8.

7.2. Effect of inlet water mass flow rate

The water mass flow rate has a significant effect on its cooling capacity; consequently, the impact of varying the mass flow of the incoming chilled water on the 3-fluid LAMEE's performance is examined and water is studied on the efficiency of the 3-fluid LAMEE. Fig. 9 shows the

variations of the 3 effectiveness and the moisture removal rate with the inlet water mass flow rate under different temperatures of the inlet water.

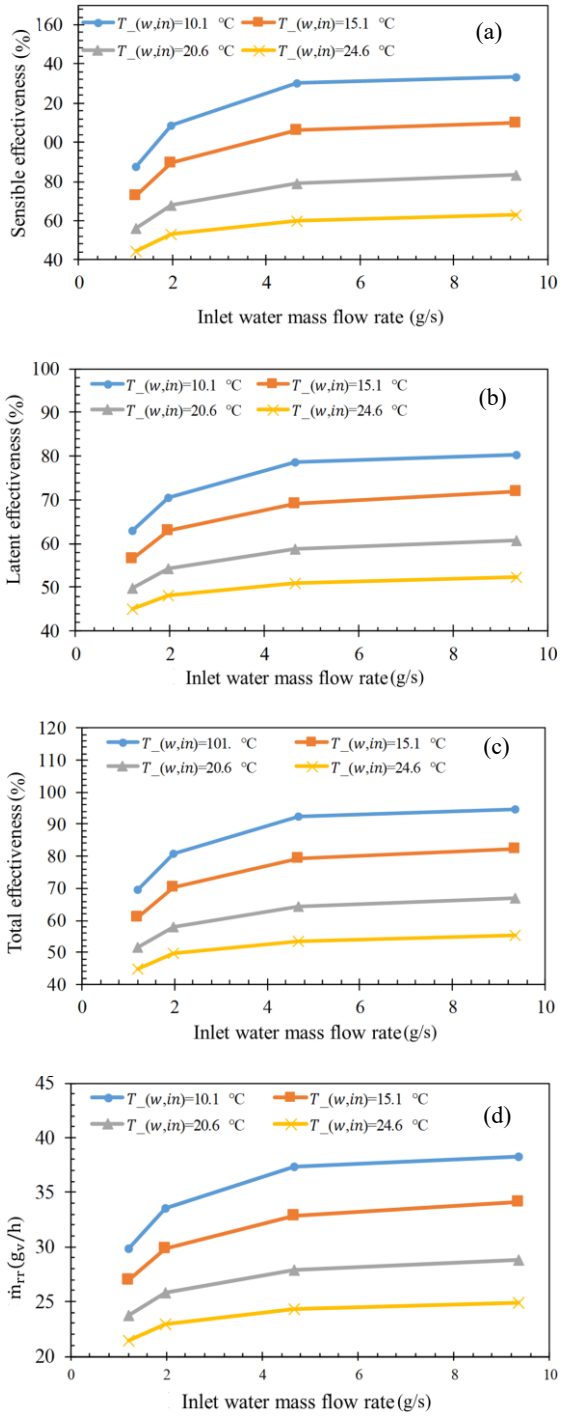

Fig. 9. Variations of effectiveness and moisture removal rate with inlet water mass flow rate at (a) Z/L=0.8, (b) Z/L=0.6, (c) Z/L=0.4, and (d) Z/L=0.2 under different inlet water temperatures.

It is evident that the latent, total, and sensible efficiency as well as the moisture rate of removal are all positively impacted through rising mass flow rate, and that these effects grow with increasing mass flow rate. Also, it can be concluded that increasing the mass flow rate at less amounts has more influence on the system performance. For instance, at $T_{w,\,in}$=20.6 °C, the sensible effectiveness increases from 56% to 68% as the mass flow rate increases from 1.22 g/s to 1.98 g/s, whereas it increases from 79% to 83% as the mass flow rate increases from 4.67 g/s to 9.35 g/s.

Fig. 10 displays the variations of temperature across the XZ plane at different Z/L under various initial freshwater mass flow rates and $T_{w,\,in}$=15.1 °C. The temperature of the center of tube decreases as the inlet water mass flow rate increases, because when the mass flow rate of a fluid increases, the heat capacity rate of the fluid increases relatively. Because of that, the fluids with higher mass flow rates are able to chill the dehumidifier liquid more and consequently the airflow.

7.3. Effect of different inlet conditions of the refrigeration tubes

This section looks at how the positioning of the refrigerant tubes affects the chilling of the desiccant solution. The ideal input conditions for the tubes are then introduced to accomplish the system's maximum performance.

The regions of the channel that require further cooling are first detected by displaying the thermal variation in this dehumidifier liquid. The streamlines of the dehumidifier liquid flow are shown in Fig. 11. Before entering the main channel (horizontal part of the channel), the desiccant solution stream travels around the refrigerant tubes in the solution inlet part of the system.

Because the output temperatures of the water of the refrigeration tubes is smaller than the initial dehumidifier solution temperature, the dehumidifier solution stream is cooled by the refrigeration tubes before exiting the solution inlet header.

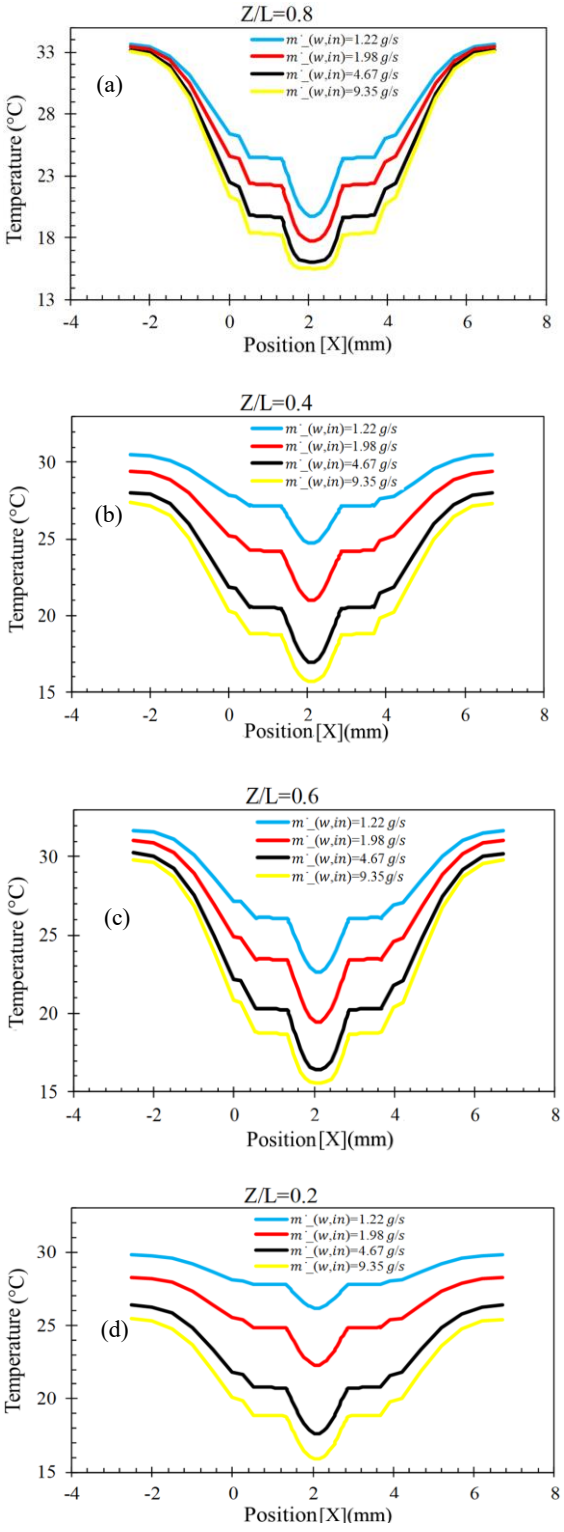

Fig. 10. Variations of temperature across the XZ plane at (a) Z/L=0.8, (b) Z/L=0.6, (c) Z/L=0.4, and (d) Z/L=0.2 under different inlet water mass flow rates.

The layers of the dehumidifier solution that entered the higher parts of the main channel were cooler than the lower levels, according to the thermal distribution of the dehumidifier solution shown in Fig. 12 and the magnified portion of Fig. 11, because they were in contact with additional refrigerated tubes in the solution inlet heading. The variations of the temperature of the cooling water are depicted in Fig. 13. Unlike the highest tubes, the lower tubes must cool the desiccant solution at a higher temperature.

Because the inlets have the same temperature and mass flow rate, the lower tubes absorb too much heat but are unable to chill the desiccant solution sufficiently, and the lower parts of the dehumidifier liquid channel remain hotter than the top parts.

Tube 7 is the final tube that the brine touches as it exits the LAMEE and the primary tube that the humidity touches as it enters the LAMEE, which adds to the maximum temperature at the outlet.

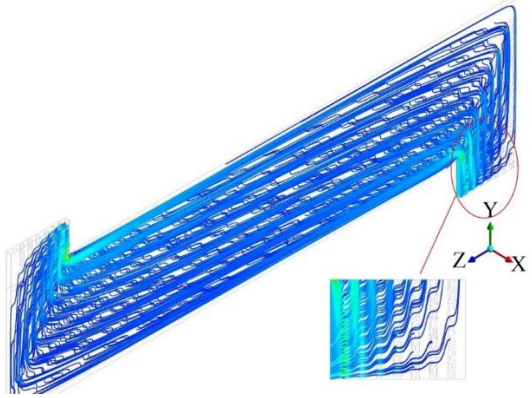

Fig. 11. Streamlines in the dehumidifier liquid channel.

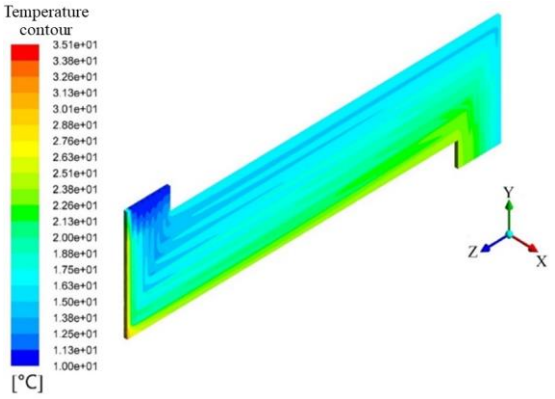

Fig. 12. Temperature contour of the desiccant throughout the desiccant solution channel.

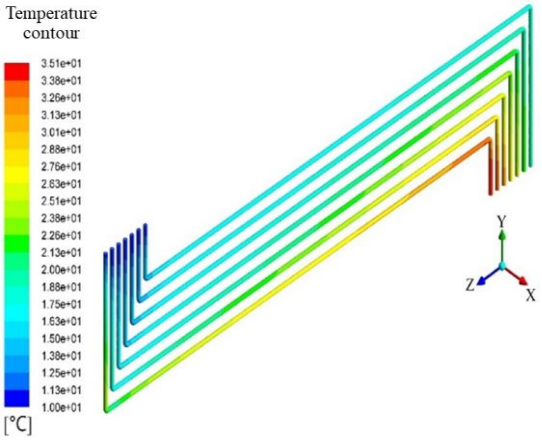

Fig. 13. Differences in cooling water temperature throughout the refrigeration tubes.

Furthermore, the 7th tube is more common in the warmer LAMEE zone (around Z/L=1) than other tubes. As a result, unlike the other tubes in the LAMEE, the water in tube 7 is unable to effectively chill the humidity and solutions. Consequently, both the temperature and vapor pressure differentials within the dehumidifier liquid and the air stream in the lower sections are less than those in the upper sections, reducing the potential for heat and moisture transfers in the lower regions. As a result, as shown in Fig. 14, air escapes the system with lower temperature and moisture via the upper regions rather than the lower parts.

Six tests are conducted to investigate the effect of different inlet conditions of the refrigeration tubes on the system performance. In section one, the effect of different inlet temperatures is studied, therefore three tests are set whose inlet mass flow rates are kept 1.98 g/s and the averages of the inlet temperatures are 15.35 °C in the 3 tests.

In test one, the inlet temperatures of the tubes decrease from 20.6 °C to 10.1 °C linearly as the height of them increases from tube seven to one.

In test two, the inlet temperatures are equal and in test three the inlet temperatures of the tubes increase from 10.1 °C to 20.6 °C linearly as their height increases from tube seven to one.

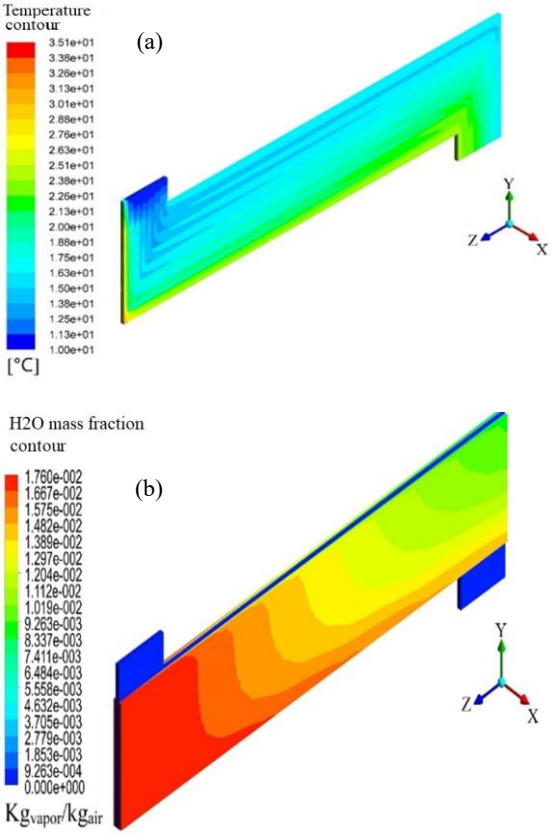

Fig. 14. Contours of (a) temperature and (b) humidity ratio, during the 3-fluid LAMEE.

As the results of the tests show in Table 4, when the temperature of the lower tubes is less than the upper tubes (test 3) the sensible, latent and total effectiveness and the moisture removal rate are maximum.

In test three, it may be determined that the lower, rather than the upper, portions of the dehumidifier liquid with the greater temperature can be cooled more; and as a result, the possibility for transfer of water and heat increases in the regions on the bottom. At test one, the reducing performance of the refrigerant tubes diminish at the key areas of the desiccant solution channel (the lower regions), therefore the system performance is less than even test two with equal temperature of the tubes inlet.

It is clear that in test three the outlet average temperature of the refrigeration tubes is less than two other tests and this type of arrangement can cool the desiccant solution more. Fig. 15 illustrates the temperature contour of 3-fluid LAMEE under the three tests.

Table 4. Results of different inlet water temperatures.

	Tubes	$T_{w,in}$ (°C)	$T_{average\_(w,in)}$ (°C)	$W_{air,out}$ (g_v/kg_a)	$T_{air,out}$ (K)	$T_{sol,out}$ (K)	$T_{w,out}$ (K)	$T_{average\_(w,out)}$ (K)	ε_{sen} (%)	ε_{lat} (%)	ε_{to} (%)	$\dot{m}_{rr}$ (g_v/h)
Test 1	Tube 1	10.1	15.35	10.99	299.5	299.9	298.9	296.3	83.5	59.5	66	28.3
	Tube 2	11.85					298.3					
	Tube 3	13.6					297.6					
	Tube 4	15.35					296.7					
	Tube 5	17.1					295.6					
	Tube 6	18.85					294.2					
	Tube 7	20.6					292.8					
Test 2	Tube 1	15.35	15.35	10.67	298.9	296.9	297.5	295.9	88.8	62.4	69.6	29.7
	Tube 2	15.35					296.9					
	Tube 3	15.35					296.4					
	Tube 4	15.35					295.9					
	Tube 5	15.35					295.4					
	Tube 6	15.35					294.9					
	Tube 7	15.35					294.6					
Test 3	Tube 1	20.6	15.35	10.21	298.5	296.3	296.1	295.6	93.2	66.6	73.8	31.6
	Tube 2	18.85					295.5					
	Tube 3	17.1					295.3					
	Tube 4	15.35					295.2					
	Tube 5	13.6					295.3					
	Tube 6	11.85					295.7					
	Tube 7	10.1					296.4					

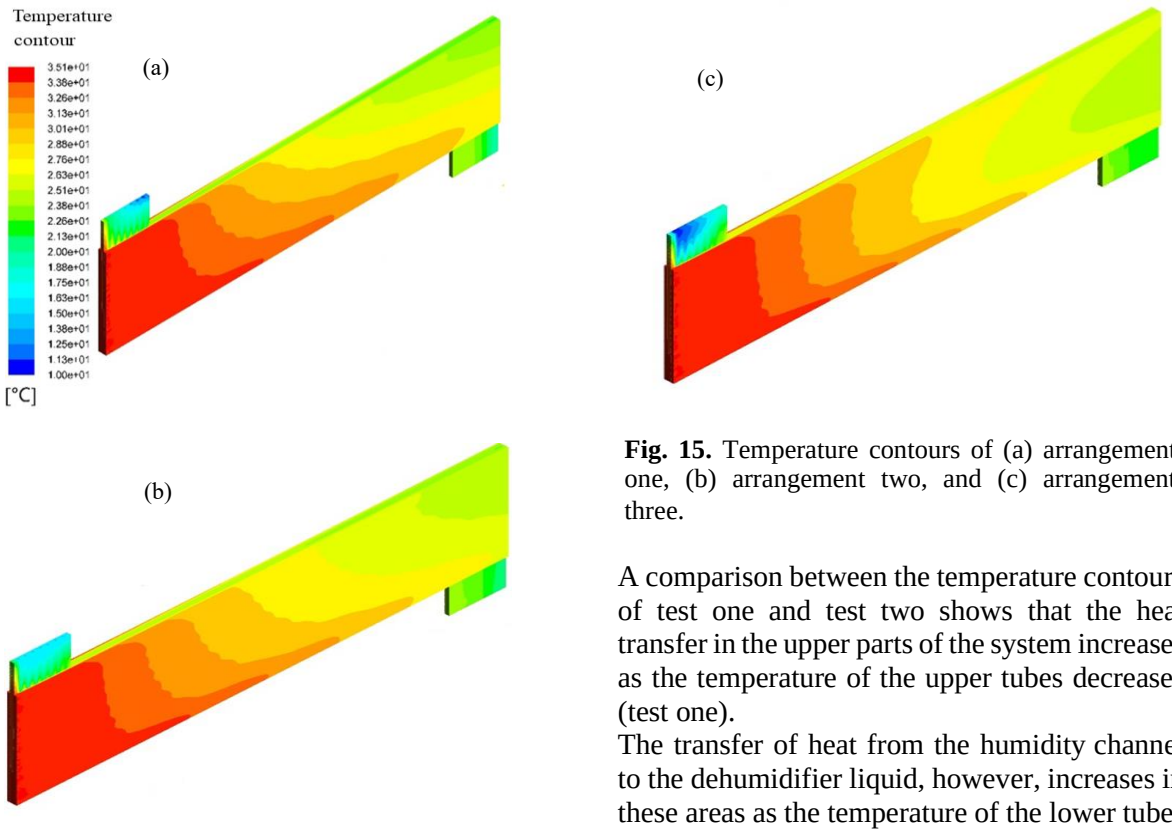

Fig. 15. Temperature contours of (a) arrangement one, (b) arrangement two, and (c) arrangement three.

A comparison between the temperature contours of test one and test two shows that the heat transfer in the upper parts of the system increases as the temperature of the upper tubes decreases (test one).

The transfer of heat from the humidity channel to the dehumidifier liquid, however, increases in these areas as the temperature of the lower tubes

drops, and the temperature of the air stream at the outlet approaches equilibrium.

In this section the effect of different inlet mass flow rates of the refrigeration tubes is investigated by three tests. The inlet temperature of the tubes is constant at 10.1℃ and three arrangements of the tubes inlet mass flow rate are set whose averages are equal.

In test four, the inlet mass flow rates of the tubes increase from 0.16 g/s to 1.34 linearly as the height of the tubes increases from tube seven to one. In test five, the inlet mass flow rates of the tubes are kept 0.75 g/s and in test six, the inlet mass flow rates of the tubes decrease from 1.34 g/s to 0.16 linearly as the height of the tubes increase from tube seven to one. Table 5 displays the results of the tests.

As the effect of the inlet mass flow rate of the cooling water was studied in section 7.2, increasing the mass flow rate of the water increases the performance of the system. The profiles of temperature and moisture ratios as well as the flow patterns generated by 3-fluid LAMEE show how the phases shift and dehumidify [31].

As a result, in test six, the mass flow rates of the lower tubes are higher than the top tubes, the cooling of the lower parts of the desiccant solution increases, and the potentials of heat and mass transfers increase in the lower parts of the 3-fluid LAMEE.

Hence the sensible, latent and total effectiveness and the moisture removal rate increase as the inlet conditions of the refrigeration tubes are arranged like test six. Fig. 16 illustrates the temperature contours of the different arrangements. It can be concluded that increasing the heat capacity rate of the lower tubes can increase their cooling capacity. Therefore, lower tubes with higher mass flow rates can be used to compensate the temperature differential among the lower parts and upper parts of the desiccant solution.

Table 5. Results of different inlet water mass flow rates.

	Tubes	$\dot{m}_{w.in}$ (g/s)	$\dot{m}_{average\_(w,in)}$ (g/s)	$W_{air,out}$ (g_v/kg_a)	$T_{air,out}$ (K)	$T_{sol,out}$ (K)	$T_{w,out}$ (K)	$T_{average\_(w,out)}$ (K)	ε_{sen} (%)	ε_{lat} (%)	ε_{tot} (%)	$\dot{m}_{rr}$ (g_v/h)
Test 4	Tube 1	1.34	0.75	9.23	295.1	296.2	297.7	290.4	125.8	75.4	89	35.7
	Tube 2	1.14					294.3					
	Tube 3	0.95					293					
	Tube 4	0.75					289.2					
	Tube 5	0.55					287					
	Tube 6	0.37					286.3					
	Tube 7	0.16					285.9					
Test 5	Tube 1	0.75	0.75	8.76	294.3	293.6	291	288.7	133.6	79.5	94.1	37.9
	Tube 2	0.75					290					
	Tube 3	0.75					289.1					
	Tube 4	0.75					288.2					
	Tube 5	0.75					287.8					
	Tube 6	0.75					287.3					
	Tube 7	0.75					287.2					
Test 6	Tube 1	0.16	0.75	8.4	293.6	293.2	287.95	288.3	140.2	82.9	98.4	39.3
	Tube 2	0.37					287.6					
	Tube 3	0.55					286.8					
	Tube 4	0.75					287.4					
	Tube 5	0.95					288.9					
	Tube 6	1.14					289.2					
	Tube 7	1.34					290.4					

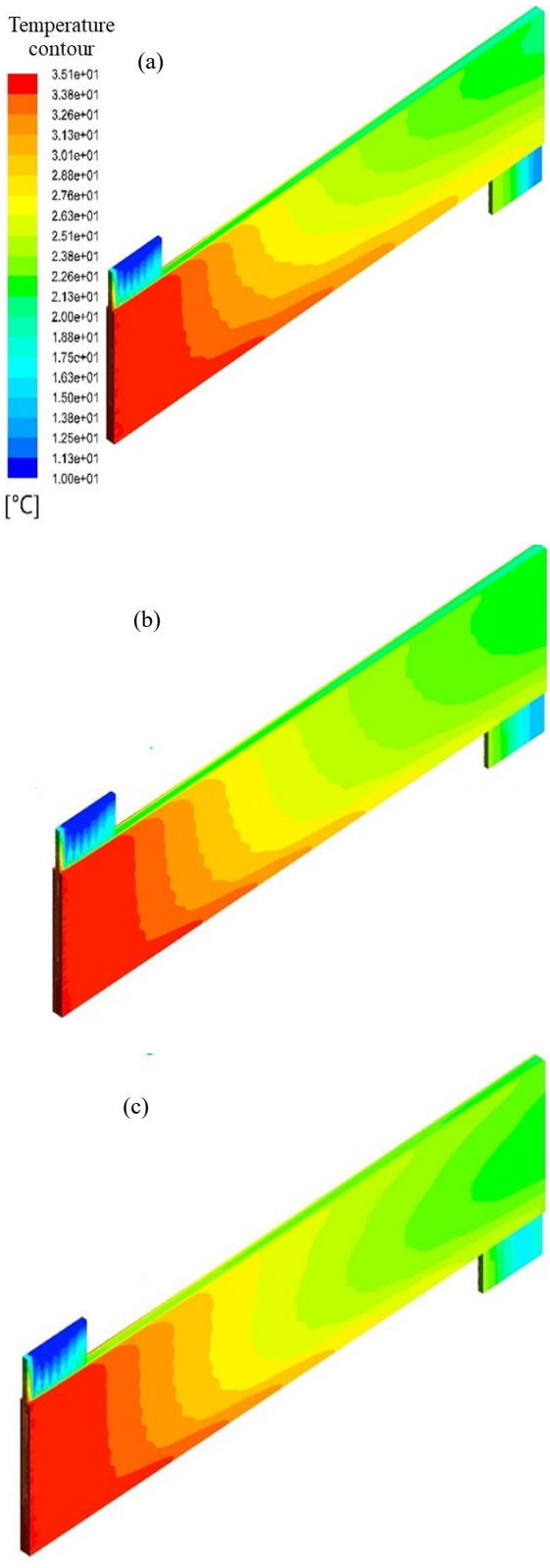

Fig. 16. Temperature contours of (a) arrangement four, (b) arrangement five, and (c) arrangement six.

8. Conclusions

The cooling capacity of the refrigerant, one of the most critical characteristics in 3-fluid LAMEEs, was thoroughly examined in this study. As a result, a 3-fluid LAMEE model was created, and the effects of incoming water conditions (temperature and mass flow rate) on system performance were explored. In addition, temperature distributions of the three fluids were displayed, and the impacts of various intake conditions to the refrigeration tubes were investigated. Six experiments were carried out to achieve the ideal inlet water conditions. The numerical investigation yielded the following results:

1. Reducing the temperature of the incoming water improves desiccant solution cooling and, as a result, system performance.
2. Increases in the incoming water mass flow rate enhance the heat capacity rate of the refrigeration tubes, which improves system performance.
3. Because the layers of desiccant solution that entered the top parts of the main channel (horizontal part of the 3-fluid LAMEE) came into contact with more cooling tubes in the solution inlet header, they were cooled more than the lower layers.
4. The lower tubes, rather than the upper tubes, must cool the desiccant solution with a higher temperature.
5. Tube 7 is in close contact with the warmest air since it is the primary tube the air comes into and the final tube where the solution comes out of. Tube 7 is also more concentrated in the LAMEE's heated area (about Z/L=1) than the remaining tubes. As a result, the fluid in tube 7 is unable to chill the air and solution, unlike the water in the rest of the LAMEE tubes.
6. The outlet air from the upper parts of the system has lower temperature and moisture rather than the lower parts.
7. In test three, the input temperatures of the tubes climb linearly from 10.1 °C to 20.6 °C, allowing the lower regions of the dehumidifier solutions to cool faster than the upper parts.

8. Increasing the mass flow rate of water in the lower tubes increases the cooling of the lower parts of the desiccant solution and consequently increases the performance of the 3-fluid LAMEE.

References

[1] A. M. Omer, " Energy, environment and sustainable development", *Renew. Sust. Energ. Rev.*, Vol. 12, No. 9, pp. 2265-2300 (2008).

[2] D. P. Wyon, " The effects of indoor air quality on performance and productivity", *Indoor Air.*, Vol. 14, No. 7, pp. 92-101 (2004).

[3] L. Pérez-Lombard, J. Ortiz and C. Pout, "A review on buildings energy consumption information", *Energy Build.*, Vol. 40, No. 3, pp. 394-398 (2008).

[4] B. Dudley, "British Petroleum. Statistical Review of World Energy", *BP*, 66nded., Vol. No. pp.1-52,(2017).

[5] A. E. Kabeel, "Dehumidification and humidification process of desiccant solution by air injection", *Energy.*, Vol. 35, No. 12, pp. 5192-5201 (2010).

[6] P. Gandhidasan and M. A. Mohandes, "Artificial neural network analysis of liquid desiccant dehumidification system", *Energy.*, Vol. 36, No. 2, pp. 1180-1186 (2011).

[7] M. R. Abdel-Salam, R. W. Besant and C. J. Simonson, "Design and testing of a novel 3-fluid liquid-to-air membrane energy exchanger (3-fluid LAMEE)", *int. J. Heat Mass Transf.*, Vol. 92, pp. 312-329 (2016).

[8] M. Tu, C. Ren, L. Zhang, J. Shao, "Simulation and analysis of a novel liquid desiccant air-conditioning system", *Appl. Therm. Eng.*, Vol. 29, No. 11-12, pp. 2417-2425, (2009).

[9] L. Z. Zhang, "Progress on heat and moisture recovery with membranes: from fundamentals to engineering applications", *Energy Convers. Manag.*, Vol. 63, pp. 173-195, (2012).

[10] M. R. Abdel-Salam, R.W. Besant and C. J. Simonson, "Sensitivity of the performance of a flat-plate liquid-to-air membrane energy exchanger (LAMEE) to the air and solution channel widths and flow maldistribution", *int. J. Heat Mass Transf.*, Vol. 84, pp. 1082-1100 (2015).

[11] M. Seyed-Ahmadi, B. Erb, C. J. Simonson and R. W. Besant, "Transient behavior of run-around heat and moisture exchanger system. Part I: Model formulation and verification", *Int. J. Heat Mass Transf.*, Vol. 52, No. 25-26, pp. 6000-6011, (2009).

[12] A. Vali, C. J. Simonson, R. W. Besant and G. Mahmood, "Numerical model and effectiveness correlations for a run-around heat recovery system with combined counter and cross flow exchangers", *Int. J. Heat Mass Transf.*, Vol. 52, No. 25-26, pp. 5827-5840 (2009).

[13] S. M. Huang, L. Z. Zhang, K. Tang and L. X. Pei, "Fluid flow and heat mass transfer in membrane parallel-plates channels used for liquid desiccant air dehumidification", *Int. J. Heat Mass Transf.*, Vol. 55, No. 9-10, pp. 2571-2580 (2012).

[14] H. Jafarian, H. Sayyaadi and F. Torabi, "Numerical modeling and comparative study of different membrane-based liquid desiccant dehumidifiers", *Energy Convers. Manag.*, Vol. 184, pp. 735-747, (2019).

[15] H. Bai, J. Zhu, Z. Chen, L. Ma, R. Wang and T. Li, "Performance testing of a cross-flow membrane-based liquid desiccant dehumidification system", *Appl. Therm. Eng.*, Vol. 119, pp. 119-131, (2017).

[16] D. Storle, M. R. Abdel-salam, N. Pourmahmoud and C. J. Simonson, "Performance Of The Dehumidification Cycle Of A 3-Fluid Liquid Desiccant Membrane Air-Conditioning System MSc". *Proc. of Building Simulation 15th Conference of IBPSA*, "*International building Performance Simulation Association*" San Francisco, CA, USA,

pp. 2533–2539, (2017).
[17] A. E. Kabeel, "Dehumidification and humidification process of desiccant solution by air injection", *Energy.*, Vol. 35, No. 12, pp. 5192-5201 (2010).
[18] M. S. Alipour and N. Pourmahmoud, "Innovative method to reduce frost formation in liquid-to-air membrane energy exchangers (LAMEE) based on 3D CFD simulation", *Int. J. Refrig.*, Vol. 147, pp. 22-31, (2023).
[19] M. S. Alipour and N. Pourmahmoud, "Frost prediction based on a 3D CFD model of heat and mass transfer in a counter-cross-flow parallel-plate liquid-to-air membrane energy exchanger", *Int. J. Air-Cond. Refrig.*, Vol. 16, pp. 2063-2076, (2023).
[20] X. Song, L. Zhang, X. Zhang, "NTU m - based optimization of heat or heat pump driven liquid desiccant dehumidi fi cation systems regenerated by fresh air or return air", *Energy.*, Vol. 158, pp. 269-280 (2018).
[21] S. M. Huang, L. Z. Zhang, M. Yang, "Conjugate heat and mass transfer in membrane parallel-plates ducts for liquid desiccant air dehumidification: effects of the developing entrances", *J. Membr. Sci.*, Vol. 437, pp. 82-89 (2013).
[22] D. G. Moghaddam, P. Lepoudre, G. Ge, R.W Besant and C. J Simonson, "Small-scale single-panel liquid-to-air membrane energy exchanger (LAMEE) test facility development, commissioning and evaluating the steady-state performance", *Energy Build.*, Vol. 66, pp. 424-436 (2013).
[23] A. H. Abdel-Salam and C. J. Simonson, "Capacity matching in heat-pump membrane liquid desiccant air conditioning systems", *Int. J. Refrig.*, Vol. 48, No. 2, pp. 166-177 (2014).
[24] A. H. Abdel-Salam and C. J. Simonson, "COP evaluation for a membrane liquid desiccant air conditioning system using four different heating equipment". *Proc. of REHVA Annual Conference* "*Advanced HVAC and Natural Gas Technologies*" Riga, Latvia, pp. 125-131, (2015).
[25] A. O. Olufade and C. J. Simonson, "Detection of crystallization fouling in a liquid-to-air membrane energy exchanger", *Exp. Therm. Fluid Sci.*, Vol. 92, pp. 33-45, (2018).
[26] L. Z. Zhang, Y. Y. Wang, C. L. Wang and H. Xiang, "Synthesis and characterization of a PVA/LiCl blend membrane for air dehumidification", *J. Membr. Sci.*, Vol. 308, No. 1-2, pp. 198-206, (2008).
[27] J. I. Yoon, T. T. Phan, C. G. Moon and P. Bansal, "Numerical study on heat and mass transfer characteristic of plate absorber", *Appl. Therm. Eng.*, Vol. 25, No. 14-15, pp. 2219-2235, (2005).
[28] J. Woods and E. Kozubal, "A desiccant-enhanced evaporative air conditioner: numerical model and experiments", *Energy Convers. Manag.*, Vol. 65, pp. 208-220 (2013).
[29] E. Bartuli., T. Kůdelová and M. Raudenský, "Shell-and-tube polymeric hollow fiber heat exchangers with parallel and crossed fibers", *Appl. Therm. Eng.*, Vol. 182, pp. 116001 (2021).
[30] M. R. Conde, "Properties of aqueous solutions of lithium and calcium chlorides: Formulations for use in air conditioning equipment design", *Int. J. Heat Mass Transf.*, Vol. 43, No. 4, pp. 367-382 (2004).
[31] M. Rashidzadeh, N. Pourmahmoud and C. J. Simonson," 3D computational fluid dynamics simulation of a 3-fluid liquid-to-air membrane energy exchanger (LAMEE)", *Appl. Therm. Eng.*, Vol. 153, pp. 501-512, (2019).
[32] M. Friedlander, G. M. Dobbs, B. N. Erb, M. W. Foster, C. Garcia and R. R. Moffitt, "Method of Testing Air-to-Air Heat Energy Exchangers", *ASHRAE*, Atlanta., Vol. 8400, pp. 1-5, (2013).
[33] C. J. Simonson and R.W. Besant, "Energy wheel effectiveness: Part I-development of dimensionless groups", *int. J. Heat Mass Transf.*, Vol. 42, No. 12, pp. 2161-2170 (1999).
[34] S. M. Ghiaasiaan, *Convective heat and mass transfer*, PhD thesis, Cambridge

University Press, Cambridge, (2011).
[35] A. Vali, *Modeling a run-around heat and moisture exchanger using two counter/cross flow exchangers*, PhD thesis, University of Saskatchewan, (2009).
[36] M. Seyed Ahmadi, *Modeling the transient behavior of a run-around heat and moisture exchanger system*, PhD thesis, University of Saskatchewan, (2008).
[37] H. B. Hemingson, C. J. Simonson and R. W. Besant, "Steady-state performance of a run-around membrane energy exchanger (RAMEE) for a range of outdoor air conditions", *Int. J. Heat Mass Transf.*, Vol. 54, No. 9-10, pp.1814-1824 (2011).

How to cite this paper:

Aydin Zabihi and Nader Pourmahmoud, "A comprehensive numerical investigation of the effects of inlet operating conditions on the performance of 3-fluid liquid-to-air membrane energy exchangers,", *J. Comput. Appl. Res. Mech. Eng.*, Vol. 13, No. 2, pp. 137-156, (2024).

DOI: 10.22061/JCARME.2024.10107.2352

URL: https://jcarme.sru.ac.ir/?_action=showPDF&article=2058